applied sciences

MDPI

Article

Lateral Structure of Multi-Layer Thick Hard Roofs and Hydraulic Roof-Cutting Pressure Relief in Xiao Jihan Mine

Hui Liu [1], Lichuang Chen [2,*], Xufeng Wang [2,3], Hui Gao [1], Chenlong Qian [2] and Xuyang Chen [2]

[1] Shanxi Huadian Yuheng Coal and Electricity Co., Ltd., Yulin 719000, China; lh15236442926@126.com (H.L.); xjhgaohui@126.com (H.G.)
[2] School of Mines, China University of Mining and Technology, Xuzhou 221116, China; wangxufeng@cumt.edu.cn (X.W.); tb22020023a51@cumt.edu.cn (C.Q.); chenxuyang@cumt.edu.cn (X.C.)
[3] Jiangsu Mine Seismic Monitoring Engineering Laboratory, Xuzhou 221116, China
* Correspondence: chenlichuang@cumt.edu.cn

Abstract

This study aims to address the pronounced stress concentration in roadway-surrounding rock under conditions of multiple thick and hard roof strata at Xiao jihan coal mine, China. The work was carried out on the 13216 working mining face as the engineering background. A systematic investigation was conducted using a combination of theoretical analysis, numerical simulation, and field experiments. Under double mining disturbance, the lower thick hard roof behaves as a cantilever beam and the upper hard roof strata form a masonry beam structure, producing strong stress transfer to the roadway. The mechanical model indicates a peak stress of 28.90 MPa, 18.34 MPa higher than the in situ stress. Hydraulic roof cutting was designed at the upper thick hard roof horizon. UDEC simulations show that the vertical stress decreases from 26.10 MPa to 13.20 MPa. Field monitoring confirms pressure relief: the non-cutting zone shows a peak of 30.75 MPa, while the roof-cutting zone drops to 22.51 MPa, a 24.62% reduction. The findings of this study provide practical guidance for lateral structure regulation under similar geological and mining conditions.

Keywords: thick hard roof strata; lateral structure; mechanical model; stress evolution; hydraulic roof cutting

1. Introduction

Thick hard roof strata account for more than 30% of underground coal mining faces in China [1]. These strata are characterized by high strength and good integrity. After the mining face is recovered, the thick hard roof is unlikely to collapse promptly, forming a cantilever and masonry structure at the lower and upper positions, respectively. This structure stores significant elastic energy internally [2–4]. During the recovery of the mining face, the combined action of the lower cantilever and upper structures leads to notable stress concentration in the coal pillar of the section. The energy accumulated within the lateral structure is rapidly released after fracturing, which can easily cause large deformations, instability of the air ventilation roadway, and other strong mining pressure phenomena such as dynamic ground pressure [5–8], severely restricting safe and efficient production on the mining face. At Xiao Jihan coal mine, stress concentration under thick hard roofs has caused recurrent roadway deformation and repeated maintenance, which increases support costs and may interrupt production, highlighting the necessity of an effective pressure relief strategy.

Check for updates

Received: 24 December 2025
Revised: 17 January 2026
Accepted: 20 January 2026
Published: 22 January 2026

Copyright: © 2026 by the authors. Licensee MDPI, Basel, Switzerland. This article is an open access article distributed under the terms and conditions of the Creative Commons Attribution (CC BY) license.

Many scholars have conducted research on the fracture characteristics, stress distribution, and control measures of hard roof strata using theoretical analysis, numerical simulation, and physical modeling. In terms of the fracture characteristics of lateral structures in hard roof strata, Gao [9] analyzed the lateral fracture mode of directly overlying hard thick roof strata, revealing the mechanism of strong mining pressure in the air ventilation roadway and clarifying the stress response characteristics during mining face recovery. Lu [10] studied the fracture patterns and quantitative characteristics of thick hard roof strata in large-mining-height, full-width mining faces, unveiling the mechanism of strong mining pressure caused by multi-layer hard roof strata in full-width mining faces. Zheng [11] developed a method for identifying the non-co-operative fracture of composite critical layers in hard roof strata, revealing the induced dynamic pressure mechanism of composite critical layer thick hard roof strata. Zhao [12] analyzed the stress characteristics and stress transfer mechanisms of coal pillars under different combinations of lateral fracture locations in overlying high- and low-position thick hard strata, establishing a mechanical model for the overall structural instability load of roadway upper hard roof strata with various fracture locations. Regarding the control of roof cutting and pressure relief in thick hard roof strata, Xu [13] established a mechanical model for the fracture of hard roof strata and proposed a coordinated fracturing technique for pressure relief at the top and bottom of the mining face, as well as a layered support system involving roof anchoring, injection strengthening, and "relieve-solid" coordinated anti-dynamic pressure control technology. He [14] revealed the hydraulic fracturing pressure relief mechanism in the far and near field of the roof, proposing a method for controlling the roof through hydraulic fracturing in the far and near field. Guo [15] proposed a comprehensive pressure relief scheme combining "roof cutting blasting + pre-splitting blasting + hydraulic fracturing," based on the fracture and migration patterns of the overlying rock layers in thick coal seams. He [16] and Guo [17] revealed the hydraulic fracturing unloading mechanism of the roof and proposed a hydraulic fracturing control method for retaining the tunnel roof. Gong [18], Wang [19], and Xu [20] studied the stress transfer mechanism of the roadway using hydraulic fracturing technology, which can alter the cantilever structure of the hard roof and block the transmission of high stress to the roadway. Ren [21] proposed a layered deep-hole blasting design, consisting of "upper fracturing and middle cutting," to address the severe stress superposition caused by multi-coal seam mining. This design facilitates directional roof failure and prevents the transmission of stress to the roadway.

In summary, numerous scholars have achieved significant technical results in the fracture characteristics of cantilever structures in thick hard roof strata and hydraulic roof-cutting pressure relief technology through theoretical analysis, simulation experiments, and field practices. International studies have also shown that, under large-mining-height longwall conditions, key stratum structures and their movement modes strongly control weighting intensity and stress redistribution, providing a useful reference for understanding hard roof ground-pressure behavior [22–26].

Previous studies have provided valuable insights into longwall stratum behavior and stress redistribution, and many mechanical descriptions focus on a single key layer or simplified single-layer roof beam behavior. However, in panels with multi-layer thick hard roofs, the overlying strata may form a high-position lateral structure and transfer stress through a coupled multi-layer path, which is not sufficiently captured by single-layer idealizations (e.g., [9–12]). In addition, the linkage between field monitoring evidence (e.g., the active roof range) and the selection of a targeted pressure relief horizon is often not explicitly integrated into a unified framework. To address these issues, this study proposes a unified approach that combines (i) a microseismic-constrained roof activity range, (ii) a multi-layer thick hard roof lateral structure mechanical model for stress transfer, and (iii)

hydraulic roof-cutting pressure relief design and field verification. Comparison of existing studies and this work are provided in Table 1.

Table 1. Comparison of existing studies and this work.

Item	Prior Single-Layer Studies (e.g., [9–12])	This Study
Roof representation	Single key stratum/single-layer roof beam idealization	Multi-layer thick hard roof lateral structure
Stress transfer path	Often simplified; limited discussion of high-position structure transfer to roadway	Explicit stress transfer analysis from high-position multi-layer structure to roadway
Monitoring linkage	Monitoring evidence not explicitly coupled to model selection	Microseismic activity range used to constrain active roof range and guide cutting horizon
Pressure relief design	General presplitting/relief concepts	Hydraulic roof-cutting pressure relief with horizon selection + field validation
Main contribution	Local/single-layer mechanism	Unified framework: monitoring + multi-layer mechanics + cut-off unloading verification

This paper takes the 13216 mining face of the Xiao Jihan coal mine as the engineering background and employs a combination of theoretical analysis, numerical simulation, and field measurements. The study aims to understand the lateral cantilever structural characteristics of multi-layer thick hard roof strata, establish a cantilever mechanical model for multi-layer thick hard roof strata, reveal the stress transfer mechanism of the lateral structure, determine the optimal hydraulic cutting layer, and clarify the stress evolution characteristics of the surrounding rock in the roadway. Additionally, the hydraulic cutting pressure relief effects are validated through field measurements. This research can serve as a reference for addressing the lateral cantilever problems of thick roof strata in similar conditions through hydraulic roof cutting.

2. Overview of the Mining Face

2.1. Characteristics of Thick Hard Roof Strata

The 13216 mining face of the Xiao Jihan coal mine extracts from the No. 2 coal seam, with a burial depth ranging from 410.0 to 430.0 m, with an average of 422.3 m. The coal seam thickness ranges from 3.69 to 5.15 m, with an average of 4.97 m. The coal seam exhibits minimal overall undulation and is nearly horizontal. Overlying the coal seam are multiple layers of sandstone thicker than 10 m (as shown in Figure 1). At a depth of 3.82 m above the coal seam, there is a 21.5 m thick fine-grained feldspathic sandstone; at 51.31 m, there is an 11.47 m thick fine-grained feldspathic sandstone; at 115.3 m, a 18.32 m thick fine-grained feldspathic sandstone; and at 150.87 m, a 17.71 m thick fine-grained feldspathic sandstone. These layers are structurally intact and have high strength, due to which they are classified as hard roof strata.

The 13126 mining face has a strike length of 4630.60 m and a dip length of 318.70 m. During the excavation of the mining face, the tunnels were driven along the bottom of the coal seam using a dual-tunnel arrangement, consisting of the 13216 conveyor roadway and the 13216 auxiliary roadway. After the recovery of the mining face is completed, the auxiliary roadway serves as the return airway for the next section of the mining face. The spatial relationship of the mining face is shown in Figure 2.

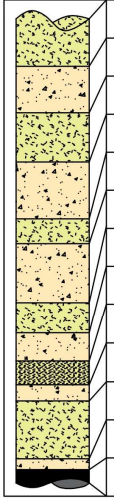
Bar chart	Layer number	Lithology	Layer thickness(m)	Distance to the coal seam(m)
	1	Fine-grained feldspathic sandstone	17.71	150.87
	2	Mudstone	17.25	133.62
	3	Fine-grained feldspathic sandstone	18.32	115.30
	4	Mudstone	21.16	94.14
	5	Fine-grained feldspathic sandstone	9.31	84.83
	6	Mudstone	22.05	62.78
	7	Fine-grained feldspathic sandstone	11.47	51.31
	8	Mudstone	11.14	40.17
	9	Medium-grained feldspathic sandstone	8.85	31.32
	10	Mudstone	6.00	25.32
	11	Fine-grained feldspathic sandstone	21.50	3.82
	12	Mudstone	3.82	0
	13	Coal seam 2	4.97	/

Figure 1. Lithostratigraphic column of the 13216 working face.

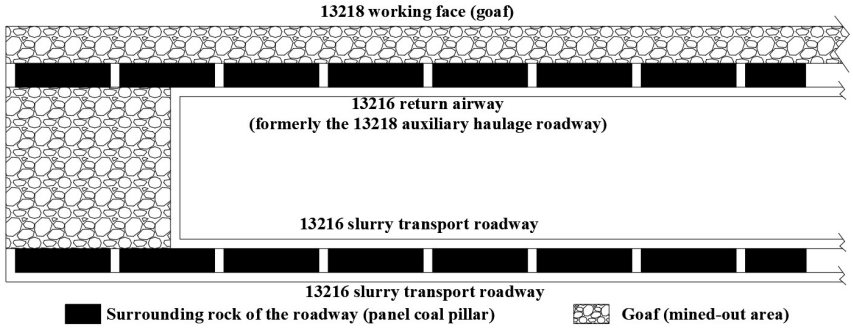


Figure 2. Positional relationship of the 13216 working face.

2.2. Roof Fracture Microseismic Monitoring

To analyze the activity range of the mining face roof, microseismic monitoring data from the 13216 mining face (as shown in Figure 3) was examined. The signals were processed to detect events, pick phase arrivals, and locate hypocenters using arrival time inversion with the site velocity model. To delineate the active roof range, only events with acceptable waveform and picking quality and reasonable spatial–temporal clustering above the working face were retained, while obvious operational interference was excluded. The main uncertainty in the resulting roof activity range arises from sensor network geometry and velocity model assumptions; therefore, the range was determined using quality-controlled events to reduce the influence of location errors. It was found that microseismic events were primarily distributed within a 60 m range above the mining face, with a general concentration within a 20 m range and the maximum reaching up to 54 m. Therefore, the roof activity of the mining face is confined to the thick hard rock layers within the 60 m range above the mining face.

Figure 4 presents the overall methodology workflow, including (1) field microseismic monitoring to delineate the active roof range, (2) mechanical modeling of stress transfer in the multi-layer thick hard roof lateral structure, (3) UDEC numerical simulation to evaluate the cut-off unloading effect of hydraulic roof cutting, and (4) field implementation and stress monitoring to verify the pressure relief performance.

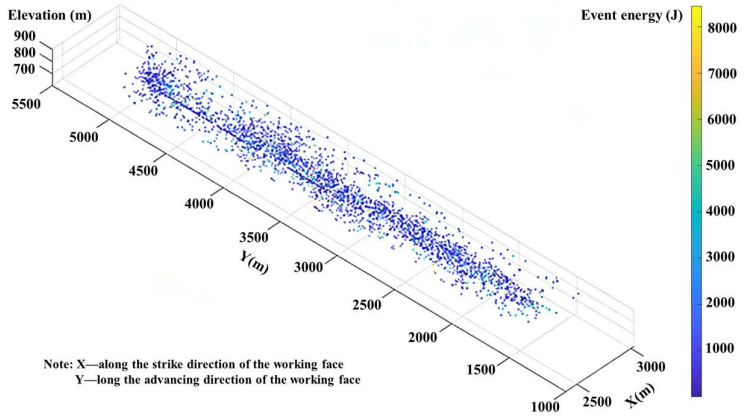


Figure 3. Distribution of microseismic events in the 13216 working face.

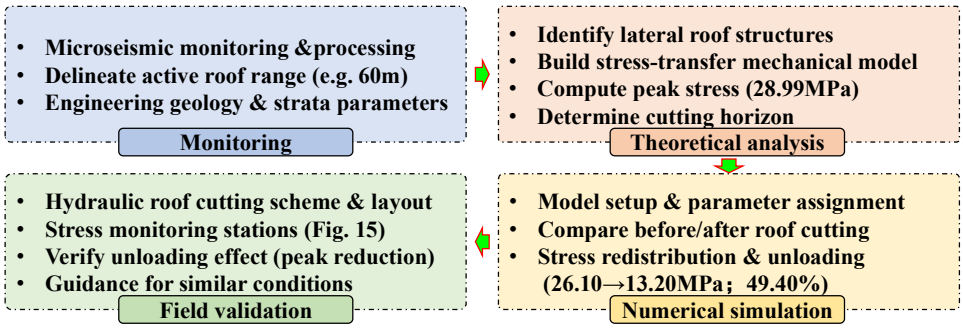


Figure 4. Overview of the study workflow.

3. Lateral Structural Characteristics and Stress Transfer of Multi-Layer Thick Hard Roof Strata

3.1. Characteristics of the Structural Form of Thick Hard Roof Strata

As the mining face progresses, the overlying thick hard roof strata successively undergo fracturing, rotation, and subsidence. The structural form of the fractured thick hard roof strata is jointly determined by the mining height and the specific layer position. Whether the thick hard rock layers enter the collapse zone and present a "cantilever beam" structure can be determined using Equation (1):

$$\Delta_i = M + \sum_{j=1}^{i-1} (1 - K_j) \times h_j > h_i - \sqrt{\frac{2q_i l_i^2}{\sigma_{ic}}} = \Delta_{i\max} \quad (1)$$

where M is the mining face height, m; K_j is the swelling coefficient of the j-th rock layer; h_i is the thickness of the rock layer, m; l_i is the maximum span of the thick hard rock layer, m; q_i is the load on the thick hard rock layer and the overlying strata, MPa; σ_{ic} is the compressive strength of the fractured block of the thick hard rock layer, MPa; Δ_i is the available rotation amount of the fractured block, m; and $\Delta_{i\max}$ is the maximum rotation amount of the fractured block, m.

The load on the thick hard rock layer and its overlying strata q_i and the maximum span l_i can be determined using the following equations:

$$(q_i)_n = E_i h_i^3 \sum_{j=i}^{n} \gamma_j h_j / \sum_{j=i}^{n} E_j h_j^3 \quad (2)$$

$$l_i = 2h_i\sqrt{\frac{\sigma_t}{3q_i}} \tag{3}$$

where $(q_i)_n$ is the load exerted by the n-th layer of the roof on the i-th layer, MPa; E_j is the elastic modulus of the j-th layer, GPa; and γ_j is the unit weight of the j-th layer, kN/m^3, where $j = i, i + 1, \ldots, n$.

As described in Section 2.1, the thick, hard strata above the 13216 working face correspond to Layers 1, 3, 7, and 11 in Figure 1, all of which are fine-grained feldspathic sandstone. The corresponding calculation parameters are provided in Table 2.

Table 2. Calculation parameters for failure of thick hard strata.

Layer Number	Distance from Coal Seam (m)	Thickness (m)	Tensile Strength (MPa)	Compressive Strength (MPa)	Elastic Modulus (GPa)
1	150.87	1.08	4.52	47.16	13.76
3	115.30				
7	51.31	1.10			
11	3.82				

By substituting the parameters from Table 2 into Equations (1)–(3), the maximum span l_i, available rotation amount Δ_i, m, and the maximum rotation amount Δ_{imax} of the thick hard rock layer can be calculated. The fracture characteristics of the hard roof strata are then determined, as shown in Table 3.

Table 3. Structural form of multi-layer thick hard roof strata.

Layer Number	Distance from the Coal Seam (m)	Discrimination Results
1	150.87	Stable
3	115.30	Stable
7	51.31	Masonry beam
11	3.82	Cantilever beam

As shown in Table 3, the lower position of the thick hard roof at 3.82 m above the coal seam exhibits a cantilever beam structure, while the upper position at 51.31 m above the coal seam exhibits a masonry beam structure. Based on this result, the fracture structure of the multi-layer hard roof strata is illustrated in Figure 5. Figure 5 is plotted with a meter-based vertical scale consistent with the stratigraphic distances above the coal seam listed in Table 2 to provide a clear reference for the roof's structural elevation.

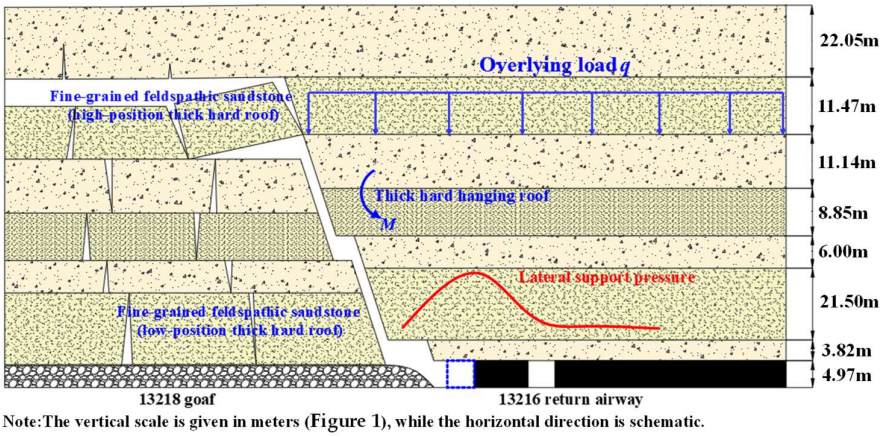


Figure 5. Lateral structural failure characteristics of multi-layer thick hard roof.

The presence of multi-layer thick hard roof strata above the 13216 mining face makes it difficult for the overlying hard roof strata to collapse promptly after the mining face is recovered, forming a long cantilever structure. This structure transmits its own load and the load of the overlying rock strata to the surrounding rock of the tunnel. At the same time, under the dual-tunnel arrangement, the 13216 return airway is subjected to disturbances from both the upper and lower mining faces, especially during the recovery of the lower mining face. Due to the combined effect of lateral pressure from the upper goaf and the advanced dual support pressure from the lower mining face, the surrounding rock stress in the tunnel becomes highly concentrated. This concentration of stress can trigger tunnel instability. Therefore, it is necessary to apply pressure relief treatment to the thick hard roof strata to reduce the load transfer capacity during the recovery of the mining face, thus improving the stress environment of the surrounding rock in the tunnel.

3.2. Impact of Lateral Structure on Tunnel-Surrounding Rock Stress

To further quantify the impact of the lateral structure on the surrounding rock of the tunnel, a mechanical model for the stress transfer of multi-layer thick hard lateral structures is established [27], as shown in Figure 6. To keep the analytical model tractable, the following assumptions are used:

(1) Elastic–rigid idealization: Roof layers are treated as elastic before macroscopic failure, while the post-fracture hinged blocks are simplified as rigid bodies with idealized contacts/hinges.
(2) Equivalent uniform load: The overburden effect is represented by an equivalent uniformly distributed load based on unit weight and layer thickness (Table 2), without explicitly modeling local heterogeneity.
(3) Rotation representation: Block rotation is described by geometric compatibility using representative rotation terms to characterize the post-fracture configuration.
(4) Constant bulking coefficient: Gob filling is estimated with constant swelling coefficients K = 1.08 and 1.10 (from the cited reference).

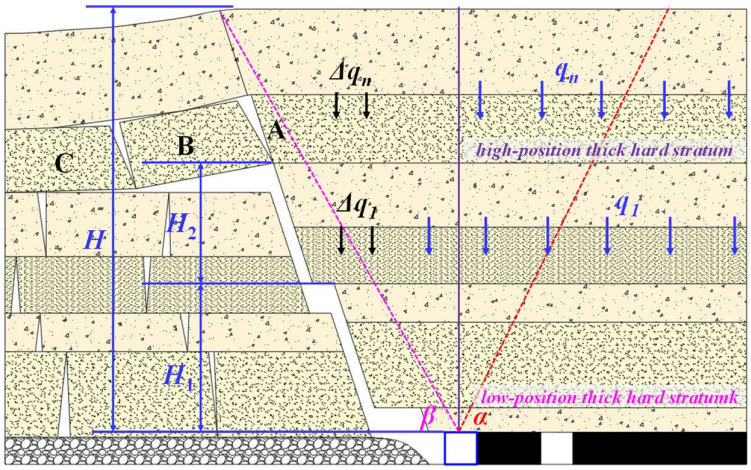


Figure 6. Stress transfer mechanical model of multi-layer thick hard lateral structure.

These assumptions mainly affect the magnitude of calculated stresses and cutting height but do not change the qualitative conclusion on the dominant stress transfer role of the high-position hinged structure.

In this model, H_1 represents the vertical height of the rock layers beneath the high-position thick hard roof, H_2 represents the total height of the high-position thick hard roof and its supporting rock layers, and H represents the overall thickness of the overlying rock

layers above the coal seam. α is the layer movement angle, and β is the fracture angle of the rock layers.

As shown in Figure 6, there are three main factors influencing the change in the surrounding rock stress of the tunnel: (i) the overlying load on the tunnel-surrounding rock (which can be considered the in situ rock stress); (ii) the additional stress transmitted by the lateral cantilever rock layers; and (iii) the force exerted by the hinged key block B. This is given by

$$\sigma = \sigma_1 + \sigma_2 + \sigma_3 \tag{4}$$

Since the overlying rock on both sides of the tunnel-surrounding rock is symmetrical, the overlying rock on one side of the tunnel-surrounding rock is taken as the object of study.

(1) Overlying Load on the Tunnel-Surrounding Rock

The overlying load on the tunnel-surrounding rock, σ_1, can be calculated using Equation (5):

$$\sigma_1 = \gamma H \tag{5}$$

where σ_1 is the unit weight, taken as 25 kN/m^3; H is the burial depth, taken as the average burial depth of 422.30 m. Thus, the self-weight stress σ_1 is calculated to be 10.56 MPa.

(2) Additional Stress Transmitted by the Lateral Cantilever Rock Layers

The additional stress σ_2 transmitted by the lateral cantilever rock layers is given by

$$\sigma_2 = \Sigma \Delta \sigma_i \tag{6}$$

where σ_i is the additional stress generated by the lateral cantilever structure of the i-th layer in the surrounding rock of the lateral tunnel. The total lateral additional stress is obtained by summing the stresses of each layer.

After the recovery of the mining face, the lateral cantilever rock stress in the goaf undergoes redistribution, but the overall state remains elastic. The bearing capacity generated by the high-position thick hard rock layers and their overlying strata can be considered as a uniformly distributed load, which can be analyzed using elastic theory.

Before face recovery, the loads of each rock layer are

$$q_i = \gamma_i h_i \tag{7}$$

After the recovery of the mining face, the load of each rock layer is as follows:

$$q'_i = \frac{\gamma_i h_i \cot \alpha + \gamma h_i \cot \beta}{\cot \alpha} \tag{8}$$

From the above, the additional load can be expressed as

$$\Delta q_i = \frac{\gamma h_i \cot \beta}{\cot \alpha} \tag{9}$$

where Δ_{qi} represents the load increment generated by the cantilever structure of the i-th layer, and h_i is the average thickness of the i-th layer. According to data from the mining company, the average collapse angle of the rock layer is 55°, and the average layer movement angle is 75°.

The load increment σ_2 generated by the cantilever portion of the overlying rock layers is given by

$$\sigma_2 = \sum \Delta q_i = \frac{\gamma \sum h_i \cot \beta}{\cot \alpha} \approx 3.35\ MPa$$

(3) Force Exerted by the Hinged Key Block

The key blocks *A*, *B*, and *C*, which are jointly supported by the tunnel-surrounding rock and the gangue, primarily undergo rotational deformation. After rotation, adjacent blocks generate horizontal thrust due to mutual compression, resulting in shear resistance and frictional resistance at the contact interface. These three components form a hinged structure that collectively supports the overlying rock layers. In this structure, key block B remains balanced through the hinging effect between the blocks and the support provided by the surrounding rock of the tunnel, as shown in Figure 7.

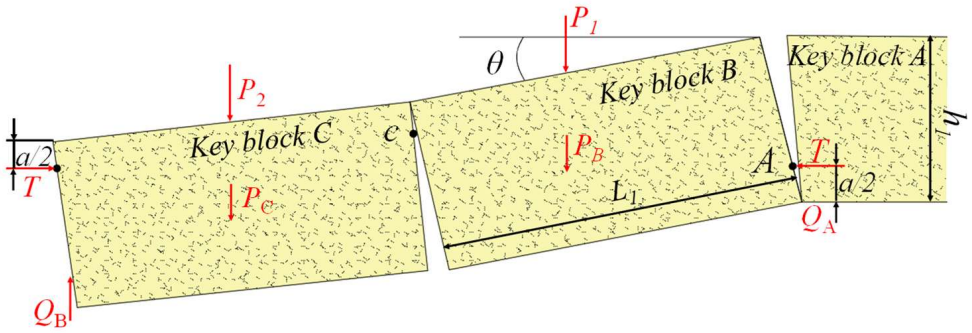


Figure 7. Mechanical structure of the hinged key block.

In the Figure 7, P_1 represents the load applied by the overlying rock stratum on key block *B*, kN/m; *T* represents the horizontal thrust, kN; Q_A represents the support force exerted by the surrounding rock of the roadway on key block *B*, kN; Q_B represents the support force exerted by the gob refuse on key block *C*, kN; L_1 represents the length of key block *B*, m; θ represents the rotation angle of key block *B*, °; and h_1 represents the thickness of the rock beam of the block, m.

A layer separation and rock block fracture occur between the fissure zone and the bending subsidence zone, leading to the interruption of the force transfer path. Therefore, the load P_1 applied by the overlying rock layers is given by

$$P_1 = L_1 \gamma_1 h_1 \tag{10}$$

where L_1 is the length of the key block, taken as the periodic step distance of 20 m; γ_1 is the average unit weight of the rock layer above key block *B*, taken as 24 kN/m^3; h_1 is the thickness of the rock layer above the key block, which is 22.05 m. Substituting these values gives $P_1 = 10564\ kN$.

The force exerted by key block *B* P_B is given by

$$P_B = L_1 \gamma_2 h_B \tag{11}$$

where γ_2 is the average unit weight of key block *B*, taken as 25 kN/m^3. Thus, $P_B = 5735\ kN$.

The spatial relationship of the rock blocks after rotation is shown in Figure 8. Based on its geometric rotational deformation characteristics, it is known that

$$2a = h_1 - L_1 \sin\theta \tag{12}$$

$$\theta = \arcsin\frac{M - \sum h_i(k_{pi} - 1)}{L_1} \tag{13}$$

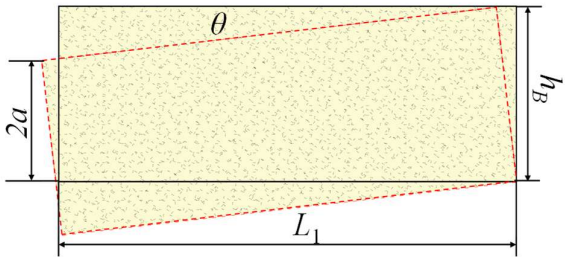


Figure 8. Geometric characteristics of the rotating rock block.

The blocks exhibit a plastic hinged relationship, so the horizontal thrust between the blocks is located at a/2, where a is the length of the rock block.

Based on the stress equilibrium principle, a mechanical analysis of the hinged structure results in the following equilibrium equation:

$$\sum M_A = 0, \sum M_C = 0, \sum F_y = 0 \tag{14}$$

The supporting force exerted by the tunnel surrounding rock on key block B can be expressed as

$$Q_A = \frac{4h_B - 3L_1 \sin\theta}{2(2h_1 - L_1 \sin\theta)}(P_1 + P_B) \tag{15}$$

From the geometric relationship and the swelling coefficient of the collapsed rock, the rotation angle of the rock mass θ is calculated to be 8.11°. Substituting this into Equation (15) yields $Q_A = 14.99\ MPa = \sigma_3$.

Based on the above analysis, the peak surrounding rock stress in the tunnel is $\sigma = 28.90\ MPa$, with a stress concentration factor of 2.74, which is an increase of 18.34 MPa compared to the in situ rock stress (the in situ rock stress is 10.56 MPa). Therefore, to improve the stress concentration in the tunnel surrounding rock caused by the lateral structure and create a favorable stress environment, hydraulic roof-cutting technology can be applied to regulate the lateral cantilever structure. This will reduce the degree of lateral support stress concentration in the surrounding rock and optimize the stress environment for the goaf recovery tunnel of the next mining face, thus enhancing the stability of the surrounding rock.

4. Hydraulic Roof-Cutting Pressure Relief Effect of Lateral Structure

4.1. Principle of Hydraulic Roof-Cutting Pressure Relief

Hydraulic roof cutting improves the stress environment of the tunnel surrounding rock by altering the lateral roof structure. After cutting, the lateral roof structure of the tunnel can be simplified as shown in Figure 9.

As shown in Figure 9, after hydraulic roof cutting and pressure relief, the cantilever structure of the low-position thick hard roof will be severed and fall into the goaf. The thinner overlying hard roof, unable to bear the overlying load, will collapse into the goaf along with the low-position thick hard roof. After the cutting effect on the high-position thick hard roof, a fracture plane is formed at the cutting position. The high-position masonry structure is transformed into a short cantilever structure. The rock blocks that collapse into the goaf will no longer exert pressure on the tunnel surrounding rock, resulting in effective relief of the surrounding rock stress and an improvement in the stability of the surrounding rock.

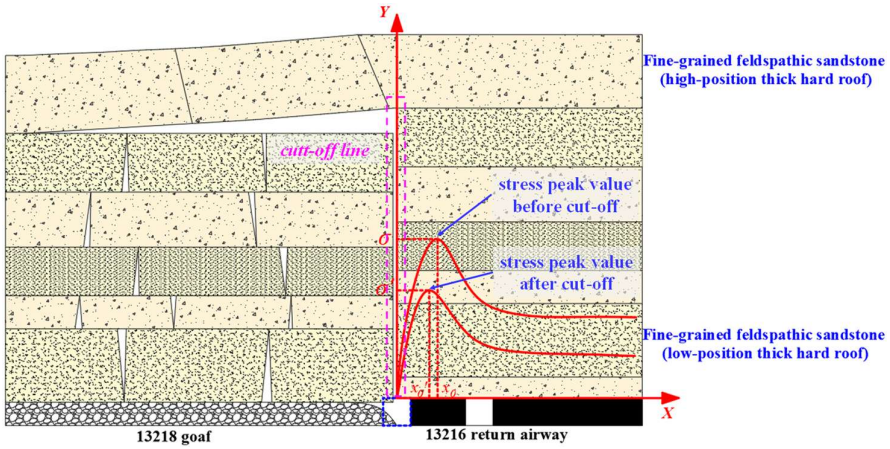


Figure 9. Lateral structural characteristics of the tunnel roof after cut-off unloading.

4.2. Determination of the Cutting Layer Position

From the analysis in Section 3.2, it is evident that among the sources influencing the change in surrounding rock stress, $\sigma_3 > \sigma_1 > \sigma_2$. This indicates that the hinged key block in the high-position masonry beam has the greatest impact on the surrounding rock of the tunnel, and therefore, it should be addressed to reduce the stress it transmits. Furthermore, the cutting height for pressure relief must be sufficient to ensure that the treated rock layers collapse and fill the goaf. This will prevent any unfilled spaces that could lead to delamination, which, when combined with the short cantilever structure after cutting, could create a new hinge, further affecting the surrounding rock. The calculation formula for hydraulic roof-cutting pressure relief is as follows:

$$H_F = \frac{M}{K-1} \tag{16}$$

where K is the bulking (swelling) coefficient of the caved rock mass. Since the broken rock expands after caving, K is generally greater than 1 [28]. K is taken as 1.08 and 1.10 in this study; M is the coal seam thickness, m.

Substituting these values, the cutting height is found to range from 49.70 to 62.12 m. By combining the roof activity range from Section 2.2 and the borehole core log, the cutting layer is determined to be at a position 51.31 m above the coal seam, corresponding to the high-position thick hard roof.

4.3. Numerical Simulation of the Hydraulic Roof-Cutting Pressure Relief Effect

Based on the geological conditions of the Xiao Jihan coal mine, the study focuses on the 13216 mining face, 13218 mining face, 13218 transport tunnel, and 13216 return airway (formerly the 13218 auxiliary roadway). The spatial relationships of the mining face and coal pillars were calculated, and based on the results, a numerical model for the hydraulic roof-cutting control of multi-layer thick hard roof strata was established using UDEC7.0 software. The surrounding rock constitutive relationship was modeled using the Mohr–Coulomb model, as shown in Figure 10. The Mohr–Coulomb model is adopted to ensure a consistent comparison of the stress transfer and cut-off unloading responses of the roadway surrounding rock before and after hydraulic roof-cutting pressure relief. However, MC is an elastic–perfectly plastic model and cannot explicitly represent the brittle post-peak behavior and fracture propagation of thick hard roof sandstone. Discontinuities (e.g., bedding/joints) and strain softening may alter local stress concentration and the extent of yielding, thereby affecting quantitative stress levels. Therefore, this study focuses

on the redistribution trend and relative unloading effect, while future work will incorporate strain-softening and explicit discontinuities to better capture post-peak failure.

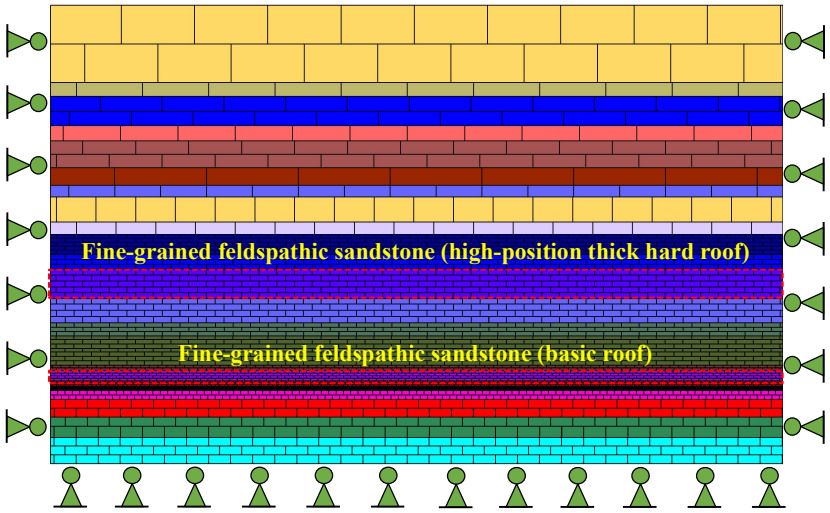


Figure 10. Numerical model establishment.

The model dimensions are 830 m × 520 m (length × height), with fixed left, right, and bottom boundaries. The velocity of the horizontal boundary and bottom boundary of the model was set to 0.

The overlying strata parameters of the working face are listed in Table 4. The numerical simulation scheme is shown in Table 5.

Table 4. Mechanical parameters of the coal and rock mass at the 13216 working face.

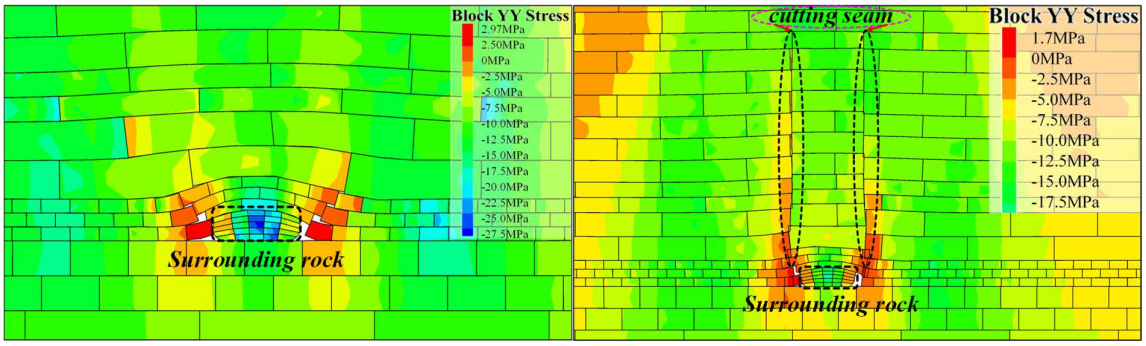
Type	Lithology	Uniaxial Compressive Strength (MPa)	Tensile Strength (MPa)	Elastic Modulus (MPa)	Cohesion (MPa)	Internal Friction Angle (°)
Main roof	Sandstone	30.64	1.60	3410	3.31	38.48
Immediate roof	Mudstone	19.9	2.90	1664	3.30	33.10
Coal		6.30	0.70	/	/	/
Floor	Mudstone	12.30	/	1729	0.94	37.50
	Sandstone	29.40	/	3489	1.54	38.20

Table 5. Numerical simulation scheme.

Scheme	Specific Content
Scheme 1	No roof cutting
Scheme 2	Roof cutting to the high-position thick hard roof, with a cutting angle of 90°

The distribution characteristics of horizontal and vertical stress in the surrounding rock of the tunnel before and after roof cutting are shown in Figures 11 and 12.

As shown in Figures 11 and 12, when no roof cutting is performed, the roof of the goaf bends and subsides under tensile stress without fracturing. The surrounding rock stress in the tunnel is clearly concentrated, with the highest concentration occurring at the center of the surrounding rock. The maximum vertical stress in the surrounding rock is 26.10 MPa, with a stress concentration factor of 2.47. When hydraulic roof cutting is applied to the high-position thick hard roof, the vertical stress in the surrounding rock of the tunnel is reduced to 13.20 MPa, and the stress concentration factor is 1.25.



(**a**) Before cut-off (**b**) After cut-off

Figure 11. Stress distribution of surrounding rock in the roadway before and after cut-off (the color scale represents stress magnitude (MPa)).

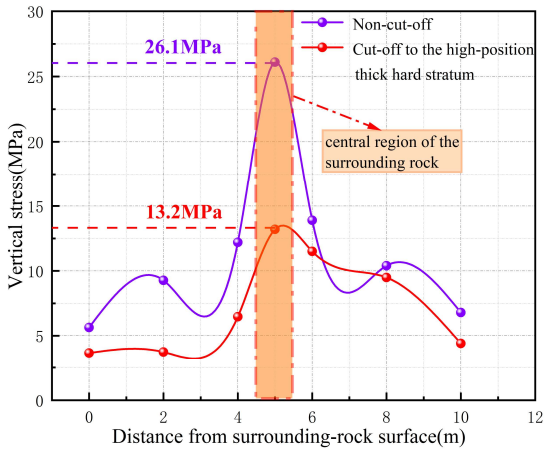


Figure 12. Distribution characteristics of vertical stress in surrounding rock before and after cut-off.

In summary, the roof-cutting technology causes the roof of the goaf to bend, subside, and fracture, leading to partial or complete collapse of the thick hard roof. This results in the transfer of stress, and the vertical stress in the surrounding rock of the tunnel is significantly reduced. When hydraulic roof cutting is applied to the high-position thick hard roof, the peak vertical stress in the surrounding rock of the tunnel decreases from 26.1 MPa to 13.2 MPa, a reduction of 49.40%. This demonstrates that cutting to the high-position thick hard roof effectively reduces the concentration of surrounding rock stress and improves the stress environment in the tunnel-surrounding rock.

5. Field Application Effects

5.1. Hydraulic Roof-Cutting Pressure Relief Scheme

Fracture holes are arranged in the tunnel roof along the strike direction from the cut-in tunnel in both headings of the 13216 working face. The holes are created using a reverse multiple fracturing method, with fracturing performed every 4 m. The layout of the fracture holes is illustrated in Figures 13 and 14.

Figure 14 illustrates the fracture hole arrangement used for hydraulic roof cutting. The fracture holes are drilled from the roof of the 13216 slurry transport tunnel and arranged regularly along the roadway; the 8 m spacing shown in the figure represents the interval between adjacent cutting holes in the layout direction. The dip/strike views indicate that the holes are organized to form a continuous cutting line/zone above the roadway roof, so that the targeted roof layer can be effectively weakened along the intended direction. Figure 14 further presents the sectional relationship between the fracture hole trajectories

and the roadway geometry, showing that the cutting holes are arranged above the roadway roof to form an effective pressure relief zone through roof cutting.

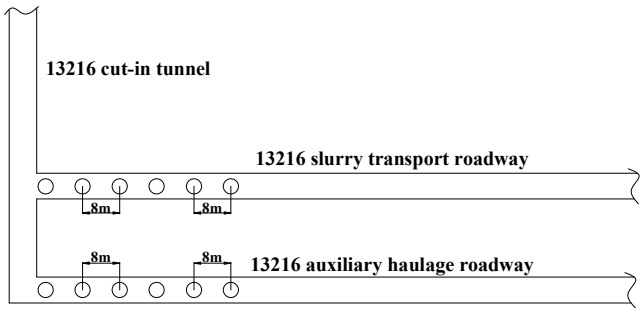
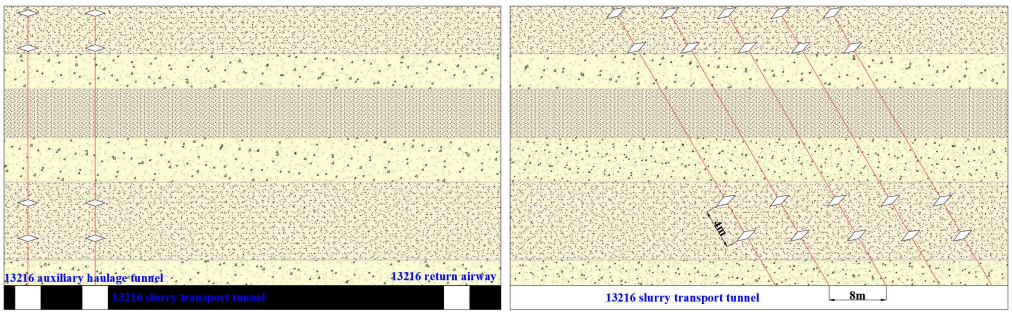


Figure 13. Schematic diagram of the fracture hole layout.



(**a**) dip (**b**) strike

Figure 14. Schematic cross-section of the fracture hole layout within the working face.

5.2. Roof-Cutting Pressure Relief Effect

The stress monitoring stations in the industrial test section were arranged as shown in Figure 15. Monitoring Station No. 1 was installed in the 13216 auxiliary haulage roadway, and the corresponding 13216 belt conveyor roadway had completed hydraulic roof cutting. The vertical stress of the roadway surrounding rock was monitored on the goaf side. Six horizontal boreholes with a diameter of 42 mm were drilled in the roadway rib at a height of 2 m above the roadway floor, and six borehole stress meters(Sourced from Shandong Zeming Energy Technology Co., Ltd., Jinan, China) were installed. The instruments were numbered 1#–6#, corresponding to installation positions at 0, 2, 4, 6, 8, and 10 m from the surrounding-rock surface of the 13216 belt conveyor roadway, respectively, with a spacing of 3 m between adjacent stress meters. Monitoring Station No. 2 was also arranged in the roof-cutting section; the instruments were numbered 7#–12#, and the layout parameters were the same as those of Monitoring Station No. 1.

To evaluate the field effect of hydraulic roof-cutting pressure relief, surrounding rock stress was monitored in the roadway section affected by the working face advance. The monitoring points were arranged along the roadway to capture the stress evolution before and after roof cutting, and the monitoring time window covered the face advance across the study section. The recorded stress data were quality-controlled and then processed to obtain representative trends, which are presented as the stress variation curve in Figure 16. It should be noted that stress readings may exhibit fluctuations and a time-dependent response; therefore, the field effect assessment is mainly based on the stabilized/representative values reflected by the monitoring records rather than instantaneous peaks.

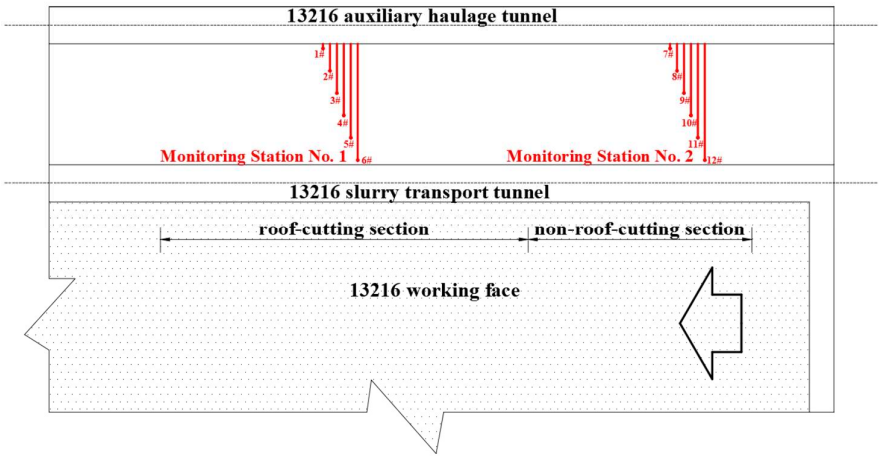


Figure 15. Layout of roadway surrounding-rock stress monitoring stations.

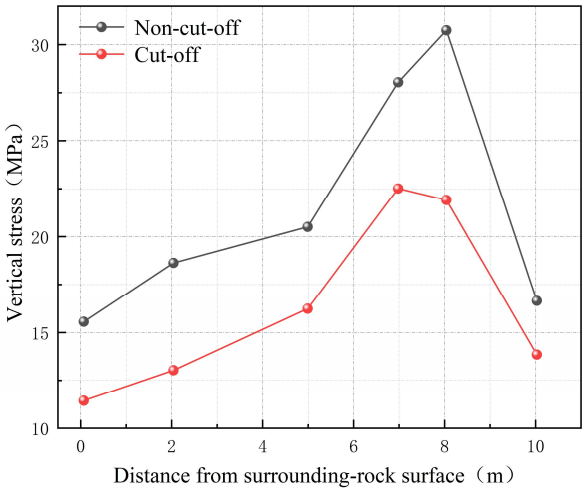


Figure 16. Vertical stress distribution curve of surrounding rock in the roadway.

As shown in Figure 16, a comparative analysis of the vertical stress in the surrounding rock at the tunnel sidewall before and after hydraulic roof cutting was conducted. In the area where hydraulic roof cutting was not applied, the peak vertical stress in the surrounding rock of the tunnel was 30.75 MPa, with an average of 21.69 MPa. In the area that underwent hydraulic roof cutting, the peak vertical stress was 22.51 MPa, with an average of 16.35 MPa. The vertical stress in the tunnel surrounding rock decreased by 24.62% after roof cutting. This demonstrates that roof cutting can effectively reduce the stress superposition caused by the multi-layer thick hard cantilever roof on the coal pillar, thereby improving the stress environment of the tunnel surrounding rock.

The peak stress level shows differences among the three approaches (28.90 MPa from the theoretical calculation, 26.10 MPa from the UDEC simulation, and 30.75 MPa from field monitoring). This discrepancy is expected because the theoretical derivation and numerical model adopt idealized assumptions (e.g., equivalent loading and simplified structural representation), while the field stress is affected by rock mass heterogeneity, discontinuities, and the spatial variability of measurement points. Therefore, this study emphasizes the consistency in the stress redistribution trend and relative unloading effect before and after hydraulic roof-cutting pressure relief, while acknowledging that absolute peak values may vary.

6. Conclusions

In this study, the structural characteristics of multi-layer thick hard roof strata and the corresponding stress transfer mechanism to the roadway were investigated for the 13216 working face at Xiao Jihan coal mine. A mechanical interpretation of the high-position "masonry beam–hinged block" structure was established, and the dominant stress contribution affecting roadway stability was clarified through stress component analysis. Based on the derived mechanical relationships and the observed roof activity range, a hydraulic roof-cutting pressure relief strategy was further proposed to weaken the stress transmission path. The main conclusions are summarized as follows:

(1) The lateral cantilever phenomenon of multi-layer thick hard roof strata and the impact of two mining disturbances lead to significantly high stress concentration in the tunnel-surrounding rock, requiring appropriate control measures. A mechanical model for stress transfer in multi-layer thick hard lateral structures was established, and it was theoretically determined that the peak stress in the tunnel-surrounding rock is 28.90 MPa, an increase of 18.34 MPa compared to the in situ rock stress.

(2) Through theoretical calculations, the position of the hydraulic roof-cutting layer was determined to be the high-position thick hard roof. Additionally, numerical simulations were used to clarify the stress distribution characteristics in the tunnel-surrounding rock before and after roof cutting. The results indicate that the vertical stress in the tunnel-surrounding rock before and after hydraulic roof cutting is 26.10 MPa and 13.20 MPa, respectively, a reduction of 49.40%. This demonstrates that hydraulic roof cutting can effectively reduce the lateral stress concentration in the surrounding rock of the tunnel.

(3) A hydraulic roof-cutting pressure relief scheme for multi-layer thick hard lateral structures was proposed and applied in field practice. The monitoring results show that in the area where hydraulic roof cutting was not applied, the peak vertical stress in the surrounding rock of the tunnel was 30.75 MPa, with an average of 21.69 MPa. In the area treated with hydraulic roof cutting, the peak vertical stress was 22.51 MPa, with an average of 16.35 MPa. The vertical stress in the surrounding rock of the tunnel decreased by 24.62% after roof cutting, leading to a significant improvement in the stress environment of the surrounding rock. The roof cutting effect was found to be effective.

7. Strengths and Limitations

(1) The study integrates field evidence with engineering decision-making, linking microseismic monitoring, mechanical analysis, and numerical simulation.

(2) The study is based on a single working face, and the findings should be validated in other mines with different roof lithologies and stress conditions.

(3) The UDEC simulation may not fully capture 3D roof structure evolution and non-uniform stress transfer, and the field validation is based on limited monitoring coverage. A discrepancy is observed between the simulated unloading effect and the field result, which may be related to rock mass heterogeneity, discontinuities, and measurement variability during face advance. Future work will employ 3D modeling and stochastic/sensitivity analyses to quantify uncertainty and improve the robustness of the hydraulic roof cutting pressure relief design.

(4) Due to incomplete archiving of the time-series raw data for each monitoring point during the field test, the standard deviation and other variability statistics cannot be reliably calculated; therefore, only peak and mean values are reported in this study. Future monitoring will implement standardized raw data archiving and quality con-

trol procedures to enable SD/uncertainty quantification and more rigorous statistical comparisons between the roof-cutting and non-cutting zones.

8. Applicability and Scope

This work is a case study of the 13216 working face (with an average burial depth of 422.3 m), and the conclusions should be interpreted within this geological scope. The proposed workflow is most applicable to large-mining-height faces with a thick hard roof where high-position lateral structures control stress transfer and where microseismic monitoring can constrain the active roof range (within 60 m in this case). For different roof lithologies (weak/laminated or strongly jointed roofs), as well as different burial depths, mining heights, and in situ stress regimes, the dominant controlling layer and stress redistribution may differ; therefore, the cutting horizon and pressure relief effectiveness should be recalibrated using site-specific monitoring and parameters.

Author Contributions: H.L.: project administration, investigation, methodology, resources, writing—original draft, writing—review and editing. L.C.: data curation, methodology, software, visualization, writing—review and editing. X.W.: supervision, writing—review and editing. H.G.: investigation, software, validation, writing—review and editing C.Q.: investigation, supervision, writing—review and editing, X.C.: investigation, methodology. All authors have read and agreed to the published version of the manuscript.

Funding: This research received no external funding.

Institutional Review Board Statement: Not applicable.

Informed Consent Statement: Not applicable.

Data Availability Statement: The data used to support the findings of this study are included and shown within the article.

Conflicts of Interest: Authors Hui Liu and Hui Gao were employed by the company Shanxi Huadian Yuheng Coal and Electricity Co., Ltd. The remaining authors declare that the research was conducted in the absence of any commercial or financial relationships that could be construed as a potential conflict of interest.

References

1. Geng, M.; Sun, J. Study on disaster mechanism of thick and hard overhanging roof and top cutting control technology. *J. Mine Autom.* **2024**, *50*, 132–141.
2. Xu, D.; Zheng, R.; Li, Y.L. Collaborative prevention and control technology of "fracture-injection-discharge-support" for thick and hard roof working face crossing faults. *Coal Eng.* **2025**, *57*, 24–33.
3. Yang, F. Research on the Breaking Law and Hydraulic Fracturing Weakening Technology of Multi-layer Hard Roof in Thick Coal Seam. Master's Thesis, Coal Science Research Institute, Beijing, China, 2025. [CrossRef]
4. Zhai, W.; Guo, Y.C.; Ma, X.C.; Li, N.L.; Zhang, P.; Ma, K.; Jing, Y.X.; Yu, H.; Li, X.T. Research on hydraulic fracturing pressure relief technology in the deep high-stress roadway for surrounding rock control. *Adv. Civ. Eng.* **2021**, *2021*, 1217895. [CrossRef]
5. Guo, W.H.; Cao, A.Y.; Wen, Y.Y.; Xue, C.C.; Lyu, G.W.; Zhao, Q. Mechanism of rockburst in stopes with typical thick roof and wide coal pillars in Ordos mining area. *J. Min. Saf. Eng.* **2021**, *38*, 720–729.
6. Gao, M.S.; Xu, D.; He, Y.L.; Zhang, Z.G.; Yu, X. Investigation on the near-far field effect of rock burst subject to the breakage of thick and hard overburden. *J. Min. Saf. Eng.* **2022**, *39*, 215–226.
7. Yang, K.; Liu, W.J.; Li, Z.H.; Liu, Q.J.; Chi, X.L.; Wei, Z. Catastrophe mechanism and prevention and control technology on soft coal mining with large inclination angle under thick and hard roof. *Coal Sci. Technol.* **2021**, *49*, 12–20.
8. Li, Y.; Chang, G.; Hu, D.; Song, W. Application of pre-splitting blasting roof-cutting pressure relief technology for roadway protection under hard roof. *Sci. Rep.* **2025**, *15*, 25458. [CrossRef]
9. Gao, X.J.; Zhang, Z.; Huang, Z.Z.; Lin, X.Y.; Xue, J.S.; Pang, L.N. Lateral fracture mode and mining stress response characteristics of overlying and thick-hard roof in deep mining well. *Rock Soil Mech.* **2024**, *45*, 2450–2461. [CrossRef]
10. Lu, Y.B.; Yan, S.H.; Zhou, K.Y.; Zhang, Z.; Wang, Y.J. Migration fracture quantitative and control of thick-hard roof in full-width working face with large mining height. *J. China Univ. Min. Technol.* **2025**, *54*, 754–769.

11. Zhang, K.G.; Yuan, L.; Zhang, P.S.; Wang, L.T. Rock bursts induced by thick-hard roof with compound key strata: Mechanisms and technical modes for prevention. *Coal Geol. Explor.* **2024**, *52*, 14−24. [CrossRef]
12. Zhao, S.K.; Zhao, Y.; Wang, Y.; Chen, Z. Experimental study on fracture mode of lateral high and low thick and hard roof in mining roadway. *Coal Sci. Technol.* **2021**, *49*, 111–120.
13. Xu, D.; Gao, M.S.; Zheng, R. Mechanism and control technology of rock burst induced by thick and hard roof breaking in simultaneous mining face. *Rock Soil Mech.* **2025**, *46*, 3219–3233.
14. He, J. Mechanism and Application of Hydraulic Fracturing Pressure Relief in Near and Far Field of Thick and Hard Roof of Coal Pillar Entry Retained. Ph.D. Dissertation, Coal Science Research Institute, Beijing, China, 2025. [CrossRef]
15. Guo, D.M.; Zhang, W.; Li, X.B.; Wang, H.K.; Zhao, Z.F.; Zhu, R.F. Comprehensive pressure relief technology of small coal-pillar roadway protection in double-roadway excavation and its application. *J. Min. Saf. Eng.* **2025**, *42*, 556–566.
16. He, M.W. Research on hydraulic fracturing treatment technology for large-area suspended roofofreuse roadway in working face with gob-side entry retaining. *China Coal* **2024**, *50*, 111–119.
17. Guo, Z.B.; Wang, H.H.; Ma, Z.M.; Wang, P.F.; Kuai, X.H.; Zhang, X.Z. Research on the transmission of stresses by roof cutting near gob rocks. *Energies* **2021**, *14*, 1237. [CrossRef]
18. Gong, G.; Liu, Z.H.; Zhang, R.F.; Wu, Z.Y.; Ma, F.T. Stress transfer mechanism and engineering practice of hydraulic fracturing roof cutting in roadway. *Saf. Coal Mines* **2025**, *56*, 165−175.
19. Wang, T.; Xu, G.Y.; Liu, L.Y.; Bai, C.Q.; Ye, W.W.; Sun, L.H. Principle and practice of hydraulic softening top-cutting and pressure relief technology in weakly cemented strata. *Front. Earth Sci.* **2024**, *12*, 1367933. [CrossRef]
20. Xu, X.D.; Zhou, Y.J.; Yang, J.; Gao, Y.B.; Zhu, C.; Wang, Y.J.; Fu, Q. A new method of mining pressure control for roof cutting in advance working face. *Eng. Fail. Anal.* **2024**, *161*, 108302. [CrossRef]
21. Ren, Z.Y.; Wang, M.X. Study on Deep Hole Blasting for Roof Cutting, Pressure Relief and Roadway Protection in Deep Multi-Coal Seam Mining. *Appl. Sci.* **2025**, *15*, 10138. [CrossRef]
22. Ju, J.F.; Xu, J.L. Structural characteristics of key strata and strata behaviour of a fully mechanized longwall face with 7.0m height chocks. *Int. J. Rock Mech. Min. Sci.* **2013**, *58*, 46–54. [CrossRef]
23. Zhang, X.Y.; Pak, R.Y.S.; Gao, Y.B.; Liu, C.K.; Zhang, C.; Yang, J.; He, M.C. Field experiment on directional roof presplitting for pressure relief of retained roadways. *Int. J. Rock Mech. Min. Sci.* **2020**, *134*, 104436. [CrossRef]
24. Islavath, S.R.; Deb, D.; Kumar, H. Development of a Roof-to-floor convergence index for longwall face using combined finite element modelling and statistical Approach. *Int. J. Rock Mech. Min. Sci.* **2020**, *127*, 104221. [CrossRef]
25. Alber, M.; Fritschen, R.; Bischoff, M.; Meier, T. Rock mechanical investigations of seismic events in a deep longwall coal Mine. *Int. J. Rock Mech. Min. Sci.* **2009**, *46*, 408–420. [CrossRef]
26. Wang, H.S.; He, M.C.; Wang, J.; Yang, G.; Ma, Z.M.; Ming, C.; Wang, R.; Zhang, W.J. Deformation mechanism and roof pre-splitting control technology of gob-side entry in thick hard main roof full-mechanized longwall caving-panel. *J. Cent. South Univ.* **2024**, *31*, 3206–3224. [CrossRef]
27. Chang, Z.C.; Wang, X.F.; Qing, D.D.; Sun, Y.X.; Yue, Y.P.; Chen, X.Y.; Wang, J.Y. Controlled reconstruction and application research of lateral overlying strata structure in high-gas mines with thick-hard roofs for a fully-mechanized top-caving face. *Heliyon* **2024**, *10*, e30705. [CrossRef]
28. Lu, Y.B.; Yan, S.H.; Fu, P.; Zhou, K.Y. Stress transfer mechanism and strong rock pressure control in the roof composite structure with a large mining height. *J. Min. Saf. Eng.* **2025**, *42*, 832–844.

Disclaimer/Publisher's Note: The statements, opinions and data contained in all publications are solely those of the individual author(s) and contributor(s) and not of MDPI and/or the editor(s). MDPI and/or the editor(s) disclaim responsibility for any injury to people or property resulting from any ideas, methods, instructions or products referred to in the content.